Stability of an Inverted Pendulum Under Nonsinusoidal Forcing

Yiwei Cheng*, Samuel Shapero, Robert Hayward

* School of Civil and Environmental Engineering, Georgia Institute of Technology, Atlanta, GA, USA

Abstract

We investigate the dynamics of an inverted pendulum subjected to Jacobi elliptic forcing both numerically and experimentally. In so doing, we hope to provide a coherent picture on stability of an inverted pendulum subjected to forcing that ranges from harmonic to nonharmonic in nature. We are able to determine the regions of stability of a sinusoidally forced inverted pendulum, with results similar to earlier literature. Most importantly, we have numerically and experimentally shown that varying the eccentricity in the Jacobi elliptical function does not significantly alter the region of stability of the inverted pendulum.

1. Introduction

The pendulum is a paradigm of contemporary nonlinear dynamics. The simple pendulum only has one stable state: the vertically down orientation. However, it has been shown experimentally and numerically that if gravity is modulated at a frequency greater than the natural frequency of the pendulum, three different equilibrium states are possible: (a) stationary vertically down, (b) stationary vertically up and (c) continuous rotation either clockwise or counterclockwise. Several authors have discussed the inverted pendulum theoretically [1,2,3]. Through numerical simulations, Blackburn et al. [1] studied the dynamics of the inverted pendulum whose pivot is subjected to harmonic vertical displacement. The authors modulated the effects of gravity on the pendulum by vertically modulating the pivot position and found that the stationary vertically up state is possible when the pivot is subjected to high frequency oscillations. They also found that beyond critical amplitude of pivot oscillation, the stable inverted state is lost and the system undergoes Hopf bifurcation leading into a flutter mode. The numerical findings of Blackburn et al [1] have been experimentally validated by Smith and Blackburn [5].

In contrast to the inverted pendulum subjected to harmonic forcing, the dynamics of an inverted pendulum subjected to nonharmonic forcing remain uncertain. For simple nonlinear oscillators such as the pendulum, the solutions are Jacobi elliptic functions. Therefore, it has been proposed that these functions be used as drivers instead of harmonic function. Sanjuan [4] forced a nonlinear pendulum with a Jacobi elliptical function and showed that it is possible to switch the periodicity of a solution by altering the waveform and periodicity of the driving function, without making alterations to the rest of the system parameters. However, to our knowledge, to date, there have been no studies that investigate the dynamics of an inverted pendulum subjected to Jacobi elliptic forcing.

We investigate the dynamics of an inverted pendulum subjected to Jacobi elliptic forcing both numerically and experimentally. In so doing, we hope to provide a coherent picture on stability of an inverted pendulum subjected to forcing that ranges from harmonic to nonharmonic in nature. Among the questions we propose to explore are: What amplitudes and frequencies of periodic forcing allow the inverted pendulum to remain upright (i.e. what are the regions of stability)? Does the region of stability change when additional harmonics are added to the forcing function? Can our theoretical findings be validated through laboratory experiments?

2. Method

2.1.1. Experimental Setup

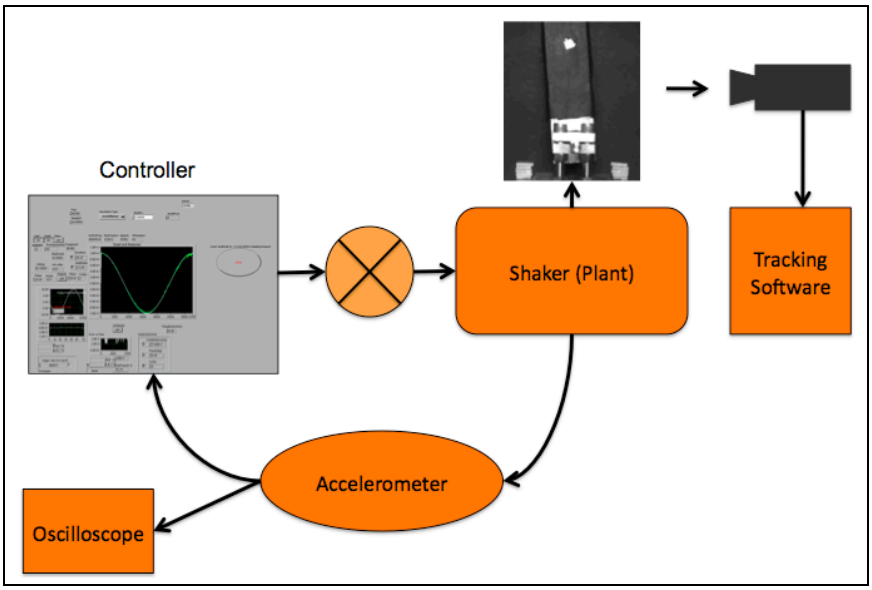

Figure 1. Schematic representation of the experimental setup.

Figure 1 describes the overall experimental setup. We control the function generator with a Labview module that allows us to specify the amplitude, frequency and eccentricity (m) of the waveform created by the function generator, thereby allowing us precise control over all parameters. The function generator is connected to an amplifier, which ultimately sends the amplified signal into the single vibrator system, VTS 500 (Vibration Test Systems, Ohio, USA). The system operates within stroke limits of 1" peak to peak, and has a maximum velocity rating of 45 in/sec, and the force limits of 500 lbf (which means we can safely drive a 500 lb load at an acceleration of 1 g). Rated frequency of the system is between 2 Hz to 5 kHz. Additional information on the specs of the system can be found here: http://vts2000.homestead.com/files/singlev.htm. VTS 500 can be programmed to produce harmonic and nonharmonic vertical displacements.

The pendulum and its pivot are mounted to an aluminum plate that is secured to a single vibrator system. The pendulum's rotation from the inverted position is limited by two rubber barriers, both about $\pi/2$ radians from the vertical. The pendulum is essentially an aluminum bar and has the following physical characteristics: $L1$ = 8.1 cm; $L2$ = 3.8 cm; radius of center of mass, r = 3.1 cm, effective radius, r^* = 7.4 cm and moment arm, I/M = 23 cm^2 (Figure 2). Natural frequency of the pendulum is calculated to be 11.5 rad/s. Accelerometer is attached to the bottom of the aluminum plate to record vertical acceleration of the plate and pendulum with time. The signals are

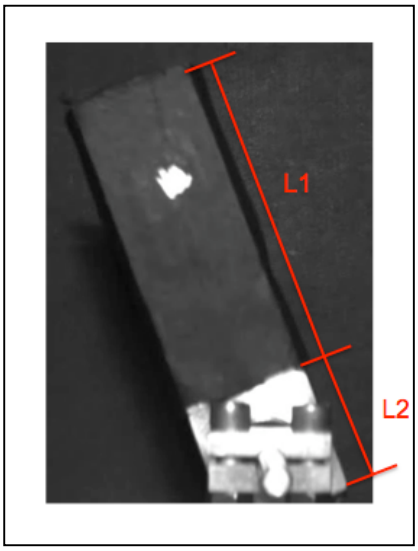

Figure 2. Picture of the pendulum used in the experiment.

also been fed to an oscilloscope to ensure that the output waveform produced by the function generator is correct.

We cover the pendulum with black color paper and painted a white dot on at the top center of the bar. The motion of the white dot represents the displacement of the pendulum in *x*-*y* plane. The motion is recorded by a high-speed camera and tracked by a point tracker program, which is written in Labview. In this case, left-right motion of the pendulum represents displacement in the *x*-plane, while up-down motion of the pendulum represents displacement in the *y*-plane.

2.1.2. Experimental Procedure

The laboratory experiment is designed to validate the results of our numerical study (described below). We experimentally determine the stability of the pendulum for values of driving frequency and acceleration that are within the physical limits of our system. We began by trying to stabilize the pendulum at a 26 Hz forcing frequency, increasing the acceleration until the pendulum was stable in the upright position. Once the inverted pendulum is stable, we perturbed it, to measure the dynamics around the fixed point, including oscillation frequency and damping. The damping coefficient of the system is calculated by iteratively adjusting the value of Q (Eqn 5) until the simulated displacement time series matches the observed displacement time series.

We then varied the driving frequency from 20 to 50Hz, and the eccentricity m from 0 to 0.999. At each node, we first attempted to stabilize the pendulum by setting the acceleration as high as the amplifier would safely allow, then decreasing the peak acceleration until the pendulum was no longer stable. We recorded this acceleration, as well as the vertical displacement of the shaker. To test the stability of the pendulum, we perturbed it gently when it comes to the inverted position. If the pendulum returns to the inverted position or does not fall over during the period of observation (~ 1 - 2 min), we classify the node as stable.

2.2.1. Model Structure

General equation of motion for a pendulum subjected to vertical harmonic forcing is:

$$I\frac{\partial^2\theta}{\partial t^2} + b\frac{\partial\theta}{\partial t} + mr[g - A\omega^2\cos(\omega t)]\sin\theta = 0 \qquad (1)$$

which describes the motion of a pendulum consisting of a mass m fixed at a distance r from a pivot which is subjected to a vertical harmonic forcing, $y = A\cos(\omega t)$ (Figure 3). θ is the angular coordinate of m measured counterclockwise from the down position. b is the damping coefficient and I is the total moment of inertia of the system. By normalizing time according to the transformation ωt --> t, Equation (1) is converted to:

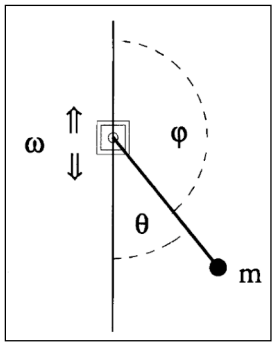

Figure 3. Schematic of a pendulum whose pivot is subjected to sinusoidal forcing.

$$\frac{\partial^2\theta}{\partial t^2}+\left(\frac{1}{\Omega Q}\right)\frac{\partial\theta}{\partial t}+\left[\left(\frac{1}{\Omega^2}\right)-\left(\frac{A}{r}\frac{mr^2}{I}\right)\cos(t)\right]\sin(\theta)=0 \qquad (2)$$

where $Q=\omega_o I/b$ and $\Omega=\omega/\omega_O$. ω_O is the undamped natural frequency and is $\omega_o^2=mgr/I$. We further simplify the equation into:

$$\frac{\partial^2\theta}{\partial t^2}+\beta\frac{\partial\theta}{\partial t}+\left[\delta-\varepsilon\cos(t)\right]\sin(\theta)=0 \qquad (3)$$

To create non-sinusoidal forcing we use the Jacobi elliptic function. Specifically, we use a cosine amplitude Jacobi elliptic function *cn(ωt, m)* of frequency *ω* and elliptic parameter *m*. There are two limits for *m*: when *m* = 0, the trigonometric function, *cos ωt* results, when *m* = 1, *sech ωt* results. Figure 2 shows how the *cn(ωt,m)* changes for some values of m.

We scale the Jacobi elliptic function such that the vertical displacement of the pivot accelerating as *cn(ωt,m)* is 2π periodic with mean of 0 and amplitude of 1. The scaling is necessary to account for the elongated period of the elliptical function when *m* > 0. The modified the Jacobi elliptic function is described as follows:

$$\alpha(t,m)=\rho(m)cn\left(\frac{T(m)}{2\pi}t,m\right) \qquad (4)$$

where *ρ(m)* is a scaling function and is:

$$\rho(m)=\frac{1}{\int_0^{\pi/2}\int_0^{t}cn\left(\frac{T(m)}{2\pi}u,m\right)dudt}$$

and *T(m)* is the period of the signal:

$$T(m)=4\int_0^{2\pi}\frac{d\theta}{\sqrt{1-m\sin^2\theta}}$$

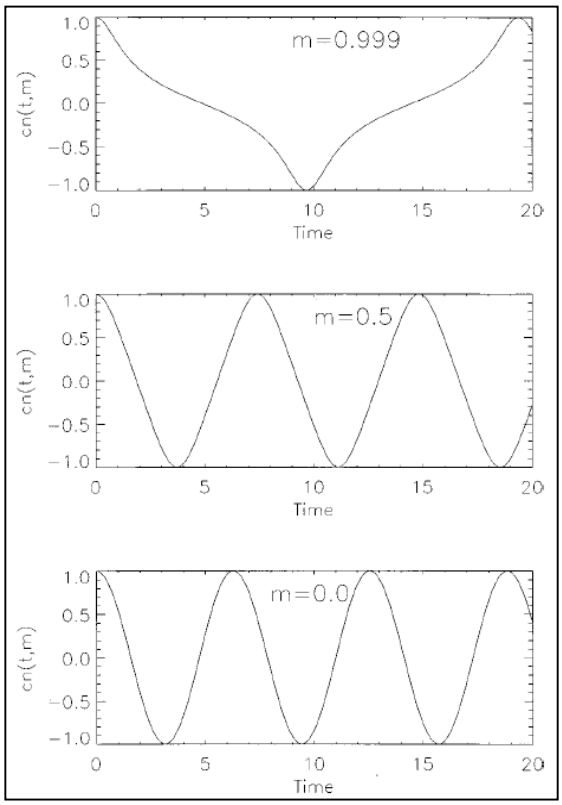

Figure 4. The variation of the cn(t,m) vs time for some values of m. The waveform and period of the wave changes as m is varied.

By replacing the sinusoidal forcing function in Eqn (3) with Eqn (4), Eqn (3) now takes the following form:

$$\frac{\partial^2\theta}{\partial t^2} + \frac{1}{Q\cdot\Omega}\frac{\partial\theta}{\partial t} + \left[\frac{1}{\Omega^2} - \varepsilon\cdot\alpha(t,m)\right]\sin(\theta) = 0 \quad (5)$$

2.2.2. Model Simulations

We first verify the stability regions for the inverted pendulum as given by Blackburn et al. [1], selecting parameters both inside and outside the region. Specifically, for a simple cosine case (i.e m = 0), we vary the relative relative amplitude ε, between 0.01 to 0.1 and the relative frequency from 15 to 55. Next, we modify the Jacobi elliptic parameter m and simulate with the same amplitude and frequency used for the simple cosine case. If any changes in stability occur as m is increased, then we will attempt to find the new boundary between the stable and unstable regions. To simulate the dynamics of the inverted pendulum, we transformed Eqn (5) into 2D system of differential equations:

$$\frac{\partial\upsilon}{\partial t} = -\frac{1}{Q\cdot\Omega}\upsilon - \left[\frac{1}{\Omega^2} - \varepsilon\cdot cn(t,m)\right]\sin(\theta)$$

$$\frac{\partial\theta}{\partial t} = \upsilon$$

Simulations are performed in Matlab, using the 4th order Runge-Kutta ODE solver, ode45. We vary three parameters in our simulations: the Jacobi Elliptic factor m, varied between 0 and 1; the relative amplitude ε, which will range from 0.01 to 0.1; and the relative frequency, which range from 15 to 55. For each point in the parameter space, we start the simulation with an initial condition of $\theta = 0$ and perform integration for 1000 periods of the forcing function. At the end of simulation, if the pendulum remains in an inverted state, the point is considered as stable. As we sweep through the parameter in a similar manner, we develop the stability diagram.

3. Results

3.1 Experimental Results

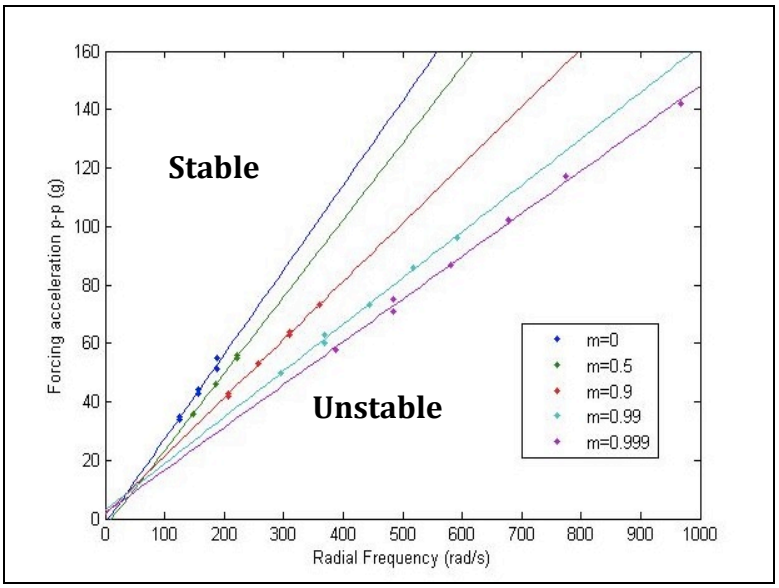

Figure 5. Scatter plot of stable points at the stability boundary as a function of forcing acceleration and radial frequency.

Figure 5 is a scatter plot of stable points at the stability boundary for each value of *m* as a function of forcing acceleration (in units of gravitational acceleration - g) and radial frequency (rad/s). Best-fit lines for each value of *m* is fitted base on the data points. For each value of *m*, the forcing acceleration required for stability is a linear function of the frequency. Results also show that the lower the value of *m*, the smaller the region of stability and vice versa.

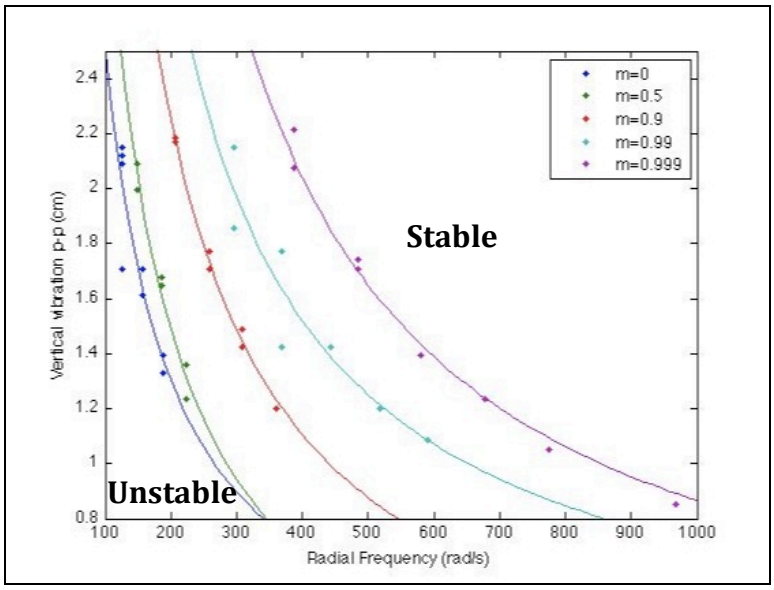

Figure 6. Scatter plot of stable points at the stability boundary as a function of vertical variation and radial frequency.

Figure 6 shows the scatter plot for the same experimental data points for each value of *m*, but as a function of vertical variation (cm) and radial frequency (rad/s). In this plot, for each value of *m*, displacement has inverse relationship with frequency.

Results also show that the lower the value of *m*, the smaller the region of stability and vice versa.

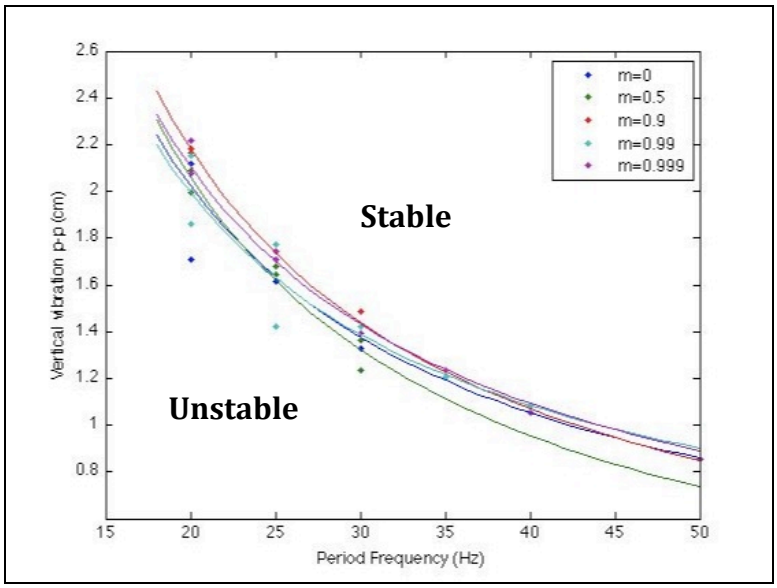

Figure 7. Scatter plot of stable points at the stability boundary as a function of vertical variation and period frequency.

Figure 7 shows the scatter plot for the same experimental data points for each value of *m*, but as a function of vertical variation (cm) and period frequency (Hz). Period frequency is equal to radial frequency/2π. In this plot, for each value of *m*, displacement has an inverse relationship with frequency. However, unlike earlier results, there are no significant differences between the regions of stability for the different values of *m*.

3.2 Simulation Results

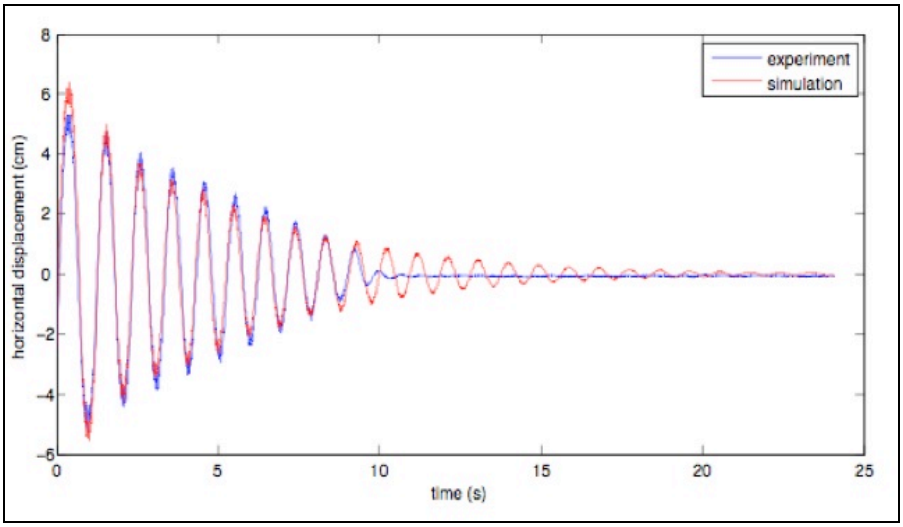

Figure 8. Simulated signal damping (red) and observed signal damping (blue).

We iteratively adjusted the value of Q in the equation of motion until a good fit is obtained between the simulated displacement and observed displacement (Figure 8). The value of Q is found to be 11 for this system.

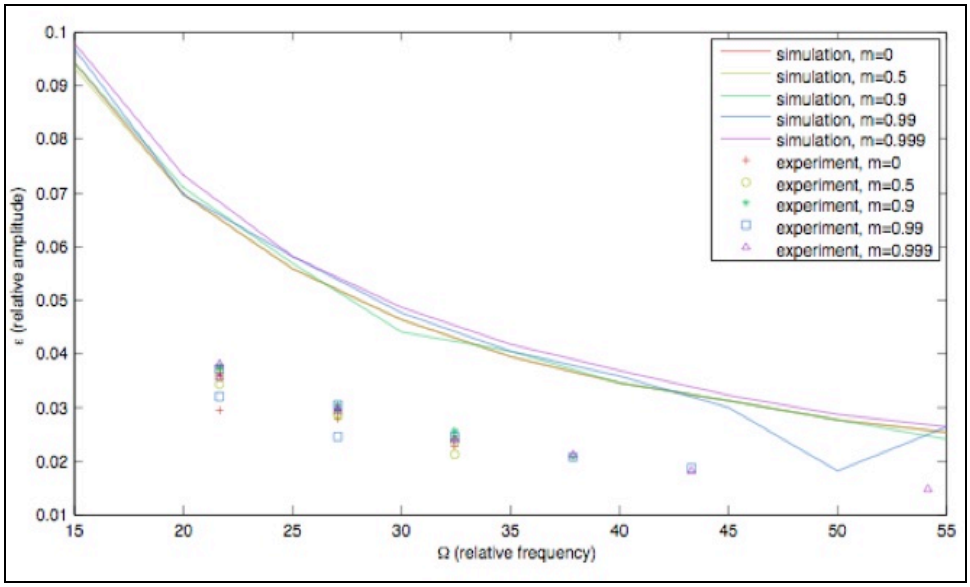

Figure 9. Stability diagram for the inverted pendulum as a function of relative amplitude and relative frequency. Lines are the simulated results and symbols represent experimental results.

Figure 9 shows the stability diagram for the inverted pendulum as a function of relative amplitude and relative frequency, based on simulation results. For each value of m, displacement has inverse relationship with frequency. Similar to experimental results, there are no significant differences between the regions of stability for the different values of m. Symbols in the diagram represent the actual data points. Results clearly show that there is a constant offset between simulation and experimental results.

4. Discussion

We have numerically and experimentally shown that the degree of eccentricity (i.e value of m) of the Jacobi elliptical function does not significantly affect the stability of the inverted pendulum. This is because it is the input acceleration that is modeled as a Jacobi elliptical function and not the input displacement. The displacement amplitude of a body accelerating as $cn(t,m)$ can be calculated by integrating the acceleration function twice. During the process of integration, energy in other harmonics gets damped out. As such, the waveform of the input displacement looks similar to a cosine wave (Figure 10). Figure 10 shows the waveform of the input acceleration (Jacobi elliptical, m=0.999), and the corresponding waveform of the input displacement obtained after scaling and integration.

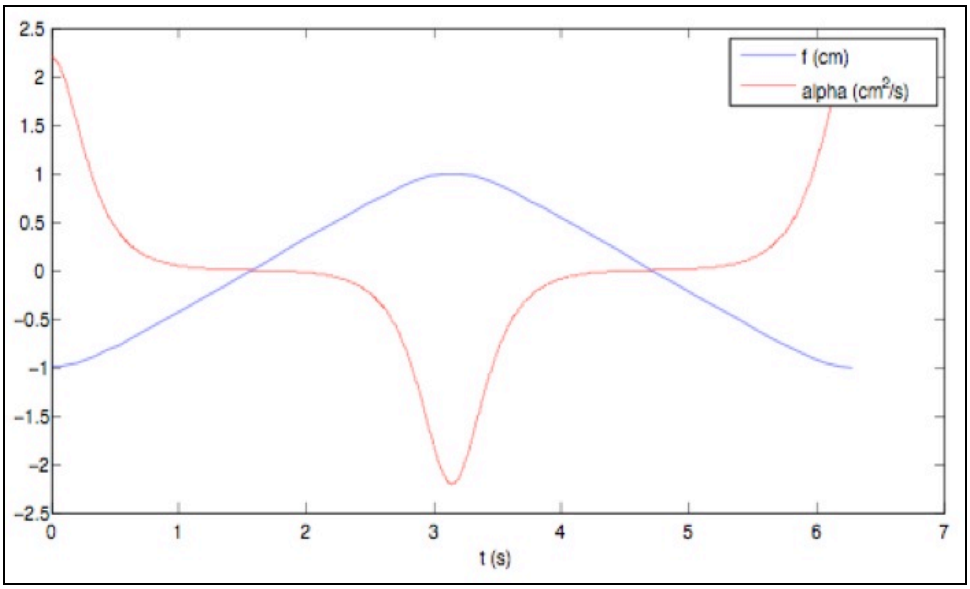

Figure 10. Waveforms of input acceleration (red) and corresponding displacement (blue).

While there are qualitative agreements between our theoretical and experimental findings, quantitative disagreements as shown clearly by the offsets between simulation and experimental results in Figure 9 suggest there are caveats to consider. In our simulations, the search for the boundary stability lacks robustness. We have only consider one initial condition for each point and have performed integration for each point for an arbitrary amount of time (1000 periods of forcing function). As such, some points, which may become stable after a long time, have been considered unstable under our current scheme. A better approach will be to take into consideration various initial conditions for each point and integrate for longer periods of time.

Damping does not seem to match qualitatively between model and experiment. As clearly shown in Figure 8, the simulated damped signal only matches the observed damped signal in amplitude and phase for the first 10 seconds. For the last 15 seconds, simulated damped signal does not match the observed damped signal in both amplitude and phase. The linear decay of the observed oscillations suggests that damping is due to a constant torque opposite to the direction of motion. By replacing the drag torque in our original equation of motion with a dynamic frictional torque of magnitude k, the equation of motion is now:

$$\frac{\partial^2\theta}{\partial t^2} + \frac{K}{\Omega^2} sign\left(\frac{\partial\theta}{\partial t}\right) + \left[\frac{1}{\Omega^2} - \varepsilon \cdot \alpha(t,m)\right]\sin(\theta) = 0$$

Where $K = k / I\omega_o^2$. Using this new model, we iteratively adjusted the value of K until the simulated signals matches the observed signals (Figure 11).

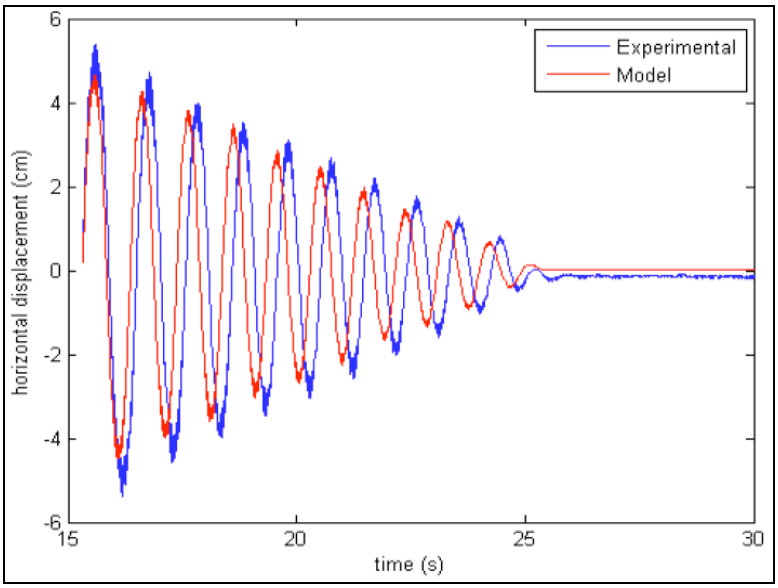

Figure 11. Simulated signal damping by the modified model (red) and the observed signal damping (blue).

The experimental stability criterion is somewhat subjective. Our criterion for stability is that the pendulum must return to the inverted position or not fall over within the period of observation (~ 1-2 min). However, it is possible that the pendulum does not fall over during the period of observation but falls over after a long period of time. This may contribute to the errors observed. A longer period of observation may reduce the errors observed.

Future work includes examining the basin of attraction both numerically and experimentally, which requires more complicated apparatus. It will also be interesting to use the Jacobi elliptical function in displacement instead of acceleration function.

5. Conclusion

We are able to determine the regions of stability of the forced inverted pendulum, with results similar to Blackburn et al. [1]. Most importantly, we have numerically and experimentally shown that varying the eccentricity in the Jacobi elliptical function does not significantly alter the region of stability of the inverted pendulum.

6. Acknowledgement

We would like to thank Andrei Savu for setting up the laboratory experiment and Nick Gravish for writing the Labview program that controlled the high-speed camera and recorded our movies, and provided invaluable debugging help. We will also like to thank Professor Goldman for his assistance and advice in getting the experiments started. Finally we would like to thank Professor Paul Umbanhowar, who constructed the shaker table and wrote the original controller program.

References

1. Blackburn, J.A., H. J. T. Smith, and N. Gronbechjensen, Stability and Hopf Bifurcations in an Inverted Pendulum. American Journal of Physics, 1992. 60(10): p. 903-908.
2. Kalmus, H.P, Inverted Pendulum. American Journal of Physics, 1970. 38(7): p. 874-878.
3. Michaelis, M.M, Stroboscopic Study of the Inverted Pendulum. American Journal of Physics, 1985. **53(11)**: p.1079-1083.
4. Sanjuan, M.A.F., Using nonharmonic forcing to switch the periodicity in nonlinear systems. Physical Review E, 1998. 58(4): p. 4377-4382.
5. Smith, H.J.T. and J.A. Blackburn, Experimental-Study of an Inverted Pendulum. American Journal of Physics, 1992. 60(10): p. 909-911.

Supplemental material, including pictures of the experimental setup, pictures of group members, bios of group members and videos of the inverted pendulum, can be found at our website http://invertpend.wordpress.com.